September 2024, Vol:2, Issue:2

International Journal of New Findings in Engineering, Science and Technology

journal homepage: *https://ijonfest.gedik.edu.tr/*

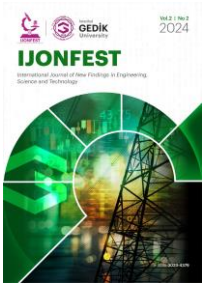

Output Parameters Estimation in A Broadband Substrate Integrated Waveguide Two- Channel T- Type Power Divider Using Adaptive Network-Based Fuzzy Inference System

Vala Tashvigh [a], Mesut Kartal [a] , Mahmood Abbasi Layegh [b*] , Aran Abbasi Layegh [c]

[a] *Department of Electronics and Communication Engineering, Istanbul Technical University, Istanbul, Turkey*
[b] *Electrical Engineering Department, Urmia University, Urmia, Iran*
[c] *Department of Electrical Engineering, Tabriz University, Iran*

Abstract

A novel substrate integrated waveguide (SIW), power divider is proposed. It consists of two channels made by SIW with the same length and width. The bandwidth of 5GHz to 14 GHz is studied here. The propagation constant of the output signals can be adjusted by only four vias in the middle of the output arms. Hence, the position of four metalized inductive vias used here are chosen as a variable ranging from 0 mm to 1 mm and they are shifted in four different positions: up, down, right and left sides. Our studies reveal that moving the vias up and down has no effects on the resonant frequency and other related parameters. However, the values of output powers and phases are changed as the vias are shifted to the right or left sides. Conventionally, artificial neural networks are tested out to obtain resonant frequency, output powers and output phases. However, they do not lead to a promising result. Finally, adaptive network-based fuzzy inference system (ANFIS) is applied in three different steps to obtain resonant frequency, output powers and output phases. As can be seen, ANFIS can determine S parameters as output signals with a high accuracy when the resonant frequency and phases of output ports are given and the average error of less than 10% can be achieved. Nevertheless, the estimation of output phases or resonant frequency results in less satisfactory results.

Keywords: Substrate integrated waveguide, Power divider, Artificial neural networks, Adaptive network-based fuzzy inference system.

1. INTRODUCTION

Creating microwave gadgets with superior quality and affordable pricing is imperative for emerging wireless communication networks. Essential elements like power dividers find extensive utility across multiple applications within microwave integrated circuits (MIC), including balanced mixers, amplifiers, phase shifters, and feed networks within antenna arrays. Significant advancements, optimizations, and theoretical breakthroughs have evolved over numerous decades [1]-[6]. Although numerous designs of N-way planar power dividers have undergone scrutiny [2]-[4], issues persist regarding unequal power distribution and accommodating dual-band applications.

Since then, a plethora of innovative methodologies have emerged to advance power dividers, encompassing dual-band performance [7], [8], bandwidth augmentation [9], and high-power utilization [10], [11]. Recent years have

https://doi.org/10.61150/ijonfest.2024020201

witnessed the emergence of numerous novel dual-band distributed-circuit power dividers, boasting both equal [13]-[15] and unequal power distributions [17], [18]. However, a predominant limitation of these dual-band power dividers lies in their restricted two-way configuration. To achieve optimal port matching and isolation across a wide frequency range, a novel coupled-line tunable Wilkinson power divider has been introduced [19]. Similarly, a groundbreaking filtering power divider boasting a wide stop band has been conceived, implementing a discriminating coupling scheme in both input and output coupling regions [20]. Reference [21] introduces an innovative substrate integrated waveguide (SIW) phase shifter, featuring phase channels crafted from SIW with uniform length but varied width. This configuration enables adjustment of the propagation constant of output signals solely by modifying the width of output arms. Previous studies have demonstrated the efficacy of Artificial Neural Networks (ANNs) in computing diverse parameters of microstrip antennas, including triangular, rectangular, and circular shapes, as well as pyramidal horn antennas [22-29]. References [30-33] utilize ANNs to accurately determine the resonant frequency of rectangular Microstrip Antennas (MSAs). Additionally, Guney and Sarikaya [34-37] successfully employ Adaptive Neuro-Fuzzy Inference System (ANFIS) to compute various parameters of rectangular, circular, and triangular MSAs. In [38], they apply the Adaptive Neuro-Fuzzy Inference System to compute the resonant frequency of electrically thin and thick rectangular microstrip antennas. ANFIS exhibits utility in modeling nonlinear functions and time series [39-40].

This paper introduces a novel substrate integrated waveguide (SIW) two-channel T-type power divider. The divider comprises two SIW channels of identical length and width. The positioning of four metalized inductive vias along the middle of the output arms serves as a variable, allowing for shifting in various directions. The study evaluates the output powers and phases for all conceivable positions of the vias and frequency variations. Notably, altering the vias' vertical position demonstrates no impact on resonant frequency, output powers, or phases. Conversely, horizontal displacement of the vias affects these parameters significantly. Subsequently, artificial neural networks are employed to predict operational frequency, output powers, and phases, albeit without precise estimations. Finally, the paper discusses simulated and measured results, concluding that the adaptive neuro-fuzzy inference system (ANFIS) represents the most suitable machine learning algorithm for such power dividers.

2. ANALYSIS AND DESIGN

Figure 1 illustrates the configuration of the envisioned power divider. The substrate integrated waveguide (SIW) is a quasi-rectangular waveguide established through periodic via-hole connections between two metal layers. In the TE mode (predominant mode), SIW behaves comparably to a traditional rectangular waveguide, exhibiting minimal leakage losses. Consequently, SIW and its analogous dielectric field waveguide possess identical TE10 mode cut-off frequencies, expressed as:

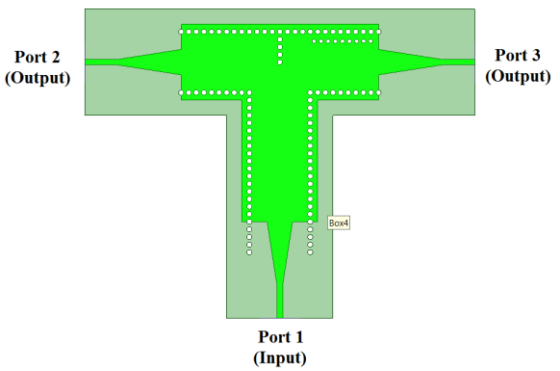

Figure 1. Structure of power divider.

$$f_c = \frac{1}{2a\sqrt{\mu\varepsilon}} \quad (1)$$

Where "a" represents the width of the rectangular waveguide equivalent to SIW, μ and ϵ denote the permittivity and permeability of said equivalent rectangular waveguide. The fundamental characteristics of SIW are approximately given as follows:

$$a = A - \frac{D^2}{0.95P} \quad (2)$$

Where a is the width of the equivalent rectangular waveguide, A is the width of SIW, D is the diameter of metalized via holes and P is the pitch between adjacent via holes as shown in figure 2.

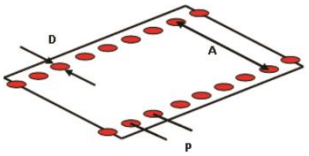

Figure 2. Rectangular waveguide integrated into a substrate.

2.1 T- Type SIW power divide with equal outputs

Substrate integrated waveguide T- type power dividers are usually appropriate for equal power division because they are symmetric and have a typical structure.

Four metalized inductive vias have been added centrally across from port 1 (input) to split the input signals equally between two output channels. Furthermore, centrally located vias act as inductive matching posts to nullify the effect of the T-junction capacitance. Hence, lower return loss can be achieved in the input. The position of these four inductive vias has an important effect in return loss and transition coefficients of the outputs. The output arms have the same width and length. Thus, the propagation constant and the phase of the output signals are expected to be the same.

The power divider design is etched onto a Rogers 4003 substrate with εr =3.55, tanδ =0.0027 featuring a substrate layer thickness of 0.508mm. At the operation frequency, the transmission coefficients at the outputs approach -3dB, accompanied by commendable return loss. Refer to figure 3 and Table I for visual and tabulated representations of the proposed power divider, respectively.

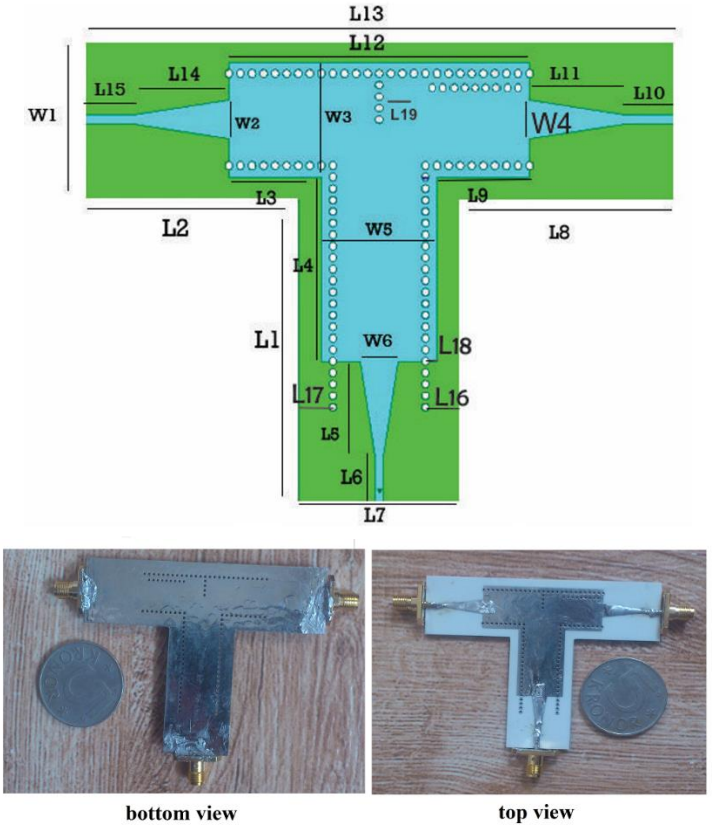

Figure 3. Geometry of the power divider.

Furthermore, the dimensions of the proposed power divider are given in details in Table 1.

Table 1. Dimensions of the proposed power divider (mm)

Parameter	mm	Parameter	mm	Parameter	mm
L1	40	L2	28	L3	12
L4	24	L5	12.5	L6	6.5
L7	21	L8	28	L9	12
L10	6.5	L11	12.5	L12	39
L13	39	L14	12.5	L15	6.5
L16	4.5	L17	4.5	L18	1.5
L19	k	W4	5	W1	21
W2	5	W3	15	W5	5

Simulation results for the prototype substrate integrated waveguide power divider are shown in figure 4. According to figure 4.(a) representing the return loss the bandwidth of 4.68 GHz is obtained from the frequency of 7.68 to 12.36. figure 4(b) illustrates that for equal signal outputs transmission coefficients for port 2 and port 3 occur at the same operation frequency. Meanwhile, figure 4.(c) shows S- parameters at the operating bandwidth.

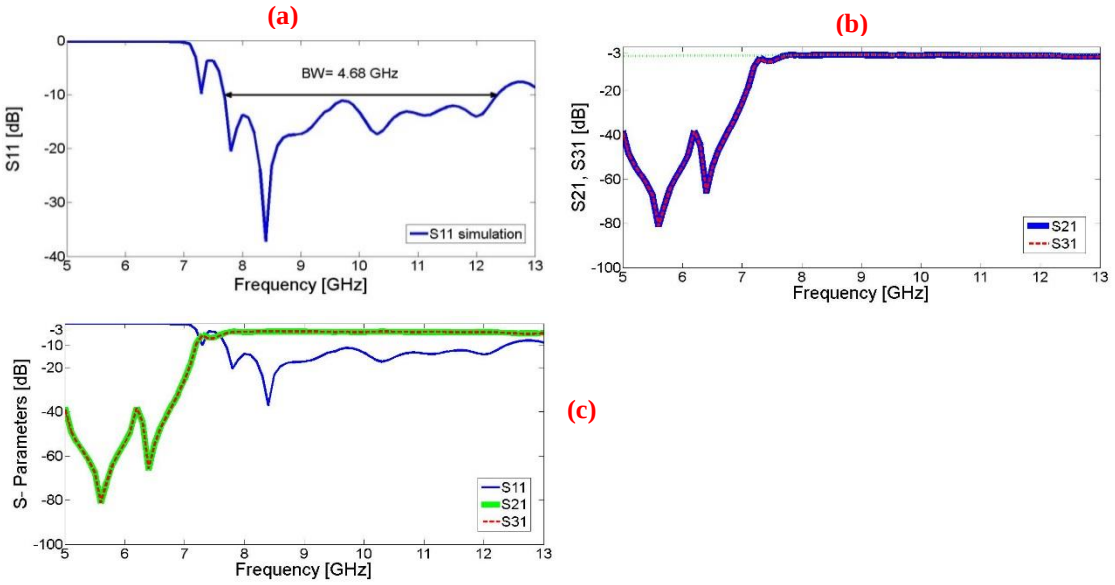

Figure 4. Simulation results for the return loss of SIW power divider (a) transmission coefficients (b) S-parameters of SIW power divider.

In figure 5, the results of both simulation and measurement of S-parameters for the whole ports are shown. It is noticeable that the simulation results of two output channels are similar.

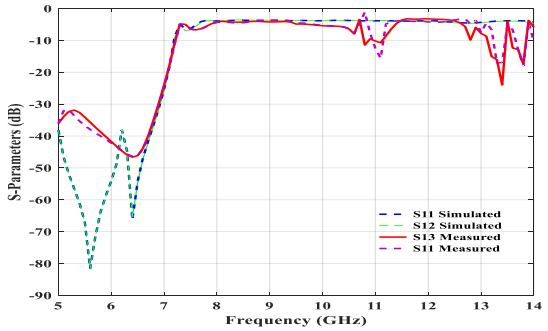

Figure 5. Results of both simulation and measurement of S-parameters for the whole ports

2.2 T- Type Unequal Power divider SIW

After optimizing the results of simulation using HFSS software, the appropriate parameters of the structure can be obtained to make desired power divider. With changing the parameter of L19= k (changing the position of central vias to left or right side) different values of power division are obtained. It is necessary that for the prototype, equal power division be applied. The values of (P) and (D) for these 4 vias are equal to 1.5 mm and 1 mm respectively.

Different values of S21 and S31 can be obtained by changing the positions of central vias to left or right hand as shown in table 2. According to table 2, when the position of central vias (L19) is shifted with the increase of 0.1 in each steps, output powers will consequently be unequal.

Table 2. S21 and S31 values for different positions

Position change (mm)	S31 (dB)	S21 (dB)	Position change (mm)	S31 (dB)	S21 (dB)
0.1	-3.6	-4	0.6	-2.8	-0.5
0.2	-3.4	-402	0.7	-2.6	-5.28
0.3	-3.3	-4.4	0.8	-2.5	-5.53
0.4	-3.16	-4.6	0.9	-2.4	-5.78
0.5	-2.9	-4.87	1	-2.3	-5.93

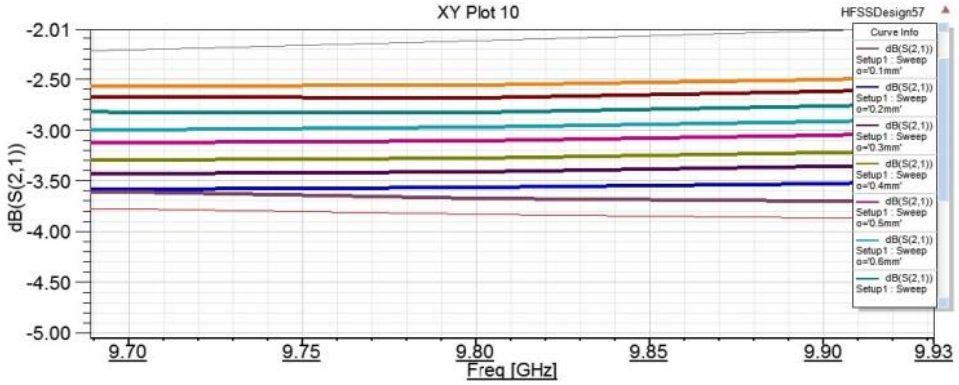

Figure 6. The value of S21 for different positions of SIW power divider

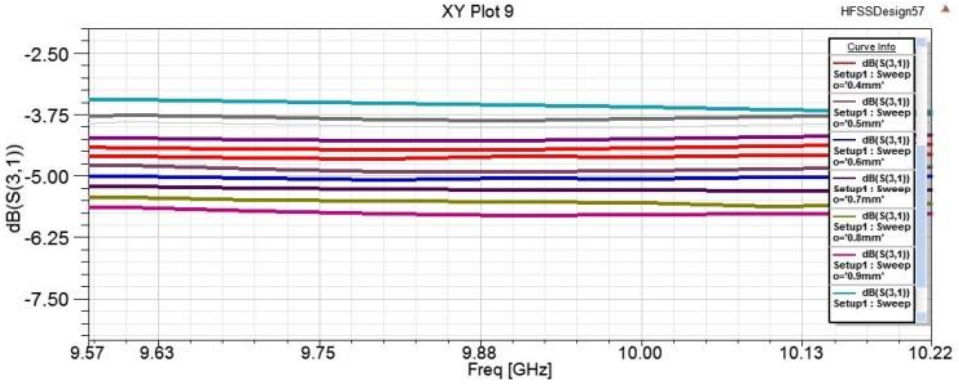

Figure 7. The value of S31 for different positions of SIW power divider

Figure 6 and figure 7 depict different values of S21 and S31 for different positions respectively. In the case that the position of central vias is shifted 1 millimeter, the value of power division in port 2 will be twice as much as that in port 3. Table 2 corroborates this matter. Figure 8 and figure 9 also show different values of power and phase outputs in port 3.

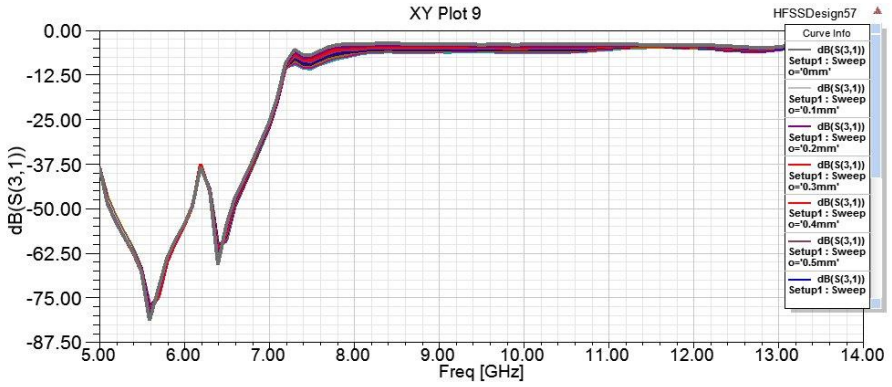

Figure 8. Output power of port 3 based on different positions of vias ranging from 5GHz to above 13 GHz

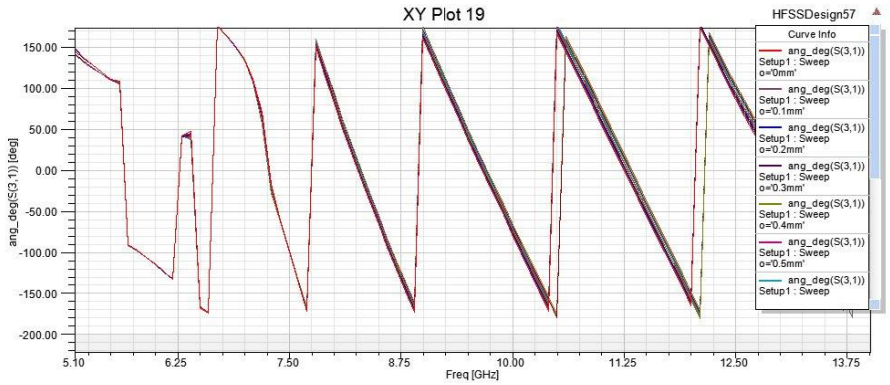

Figure 9. Output phase of port 3 based on different positions of vias ranging from 5GHz to above 13 GHz

The main purpose here is to predict the main parameters of the power divider such as resonant frequency, S-parameters and the phases of two outputs using machine algorithms based on neural networks. This study is carried out in three different steps:

a) The prediction of resonant frequency when two output powers and two output phases of the power divider are available. In addition, the position of vias is varied between 0 mm and 1mm.

b) The prediction of S21 and S31 when resonant frequency and phases of two outputs are given and the position of vias is changed between 0mm and 1mm.

c) The prediction of φ21, φ31 when resonant frequency and powers of the two outputs are given and the position of vias is changed between 0 mm and 1mm.

In the present work, artificial neural networks were employed to predict such parameters. Surprisingly, they had a very weak and unreliable performance in proceeding the process. Moreover, as can be seen in figures 10, 11 and 12, artificial neural networks represent a significant error in the recognition of the aforementioned outputs.

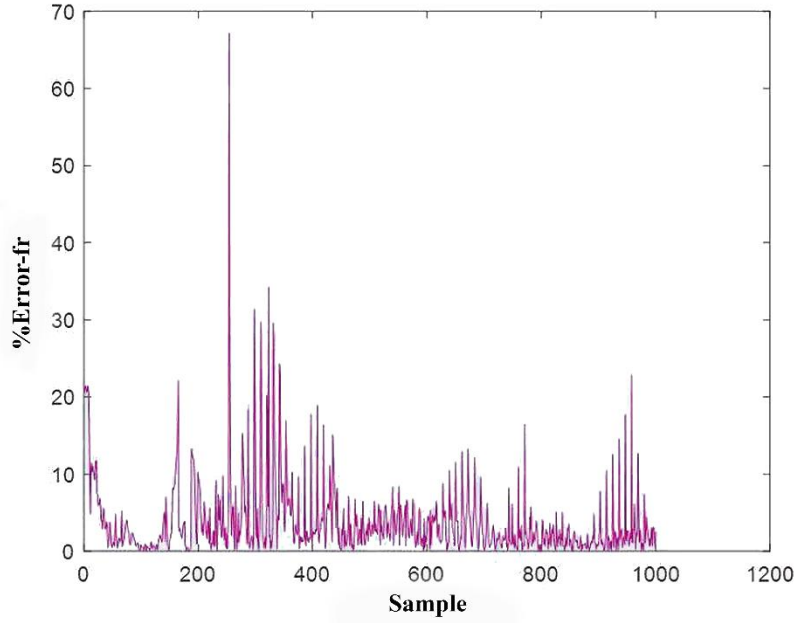

Figure 10. Error percentage of frequency estimation when S21, S31, φ21 are φ31are given as inputs.

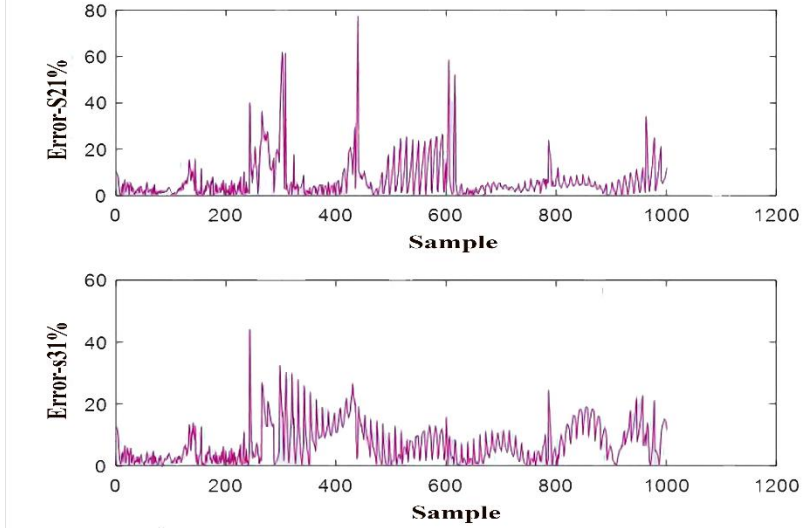

Figure 11. Error percentage of power estimation when φ21 are φ31 and resonant frequency are given as inputs

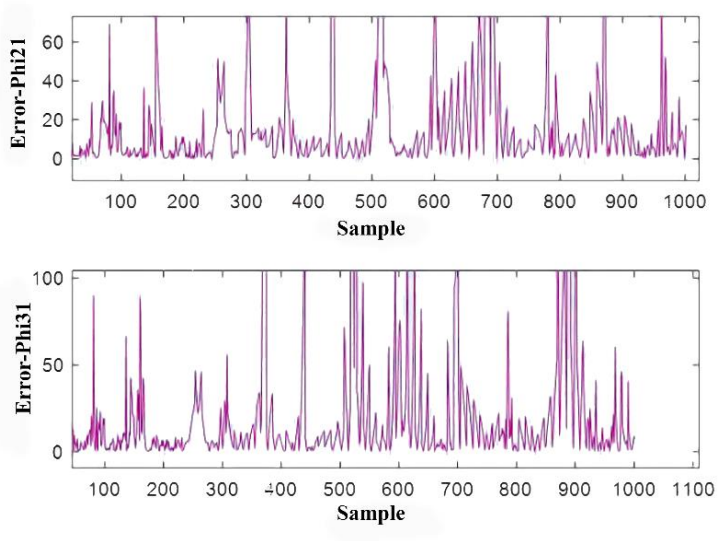

Figure 12. Error percentage of phase estimation when S21, S31 and resonant frequency are given as inputs.

2.3 Adaptive neuro fuzzy inference system

Fuzzy inference systems are alternatively referred to as fuzzy-rule-based systems, fuzzy models, fuzzy associative memories (FAM), or fuzzy controllers in controller applications. Fundamentally, a fuzzy inference system comprises five functional blocks, as depicted in Figure 13.

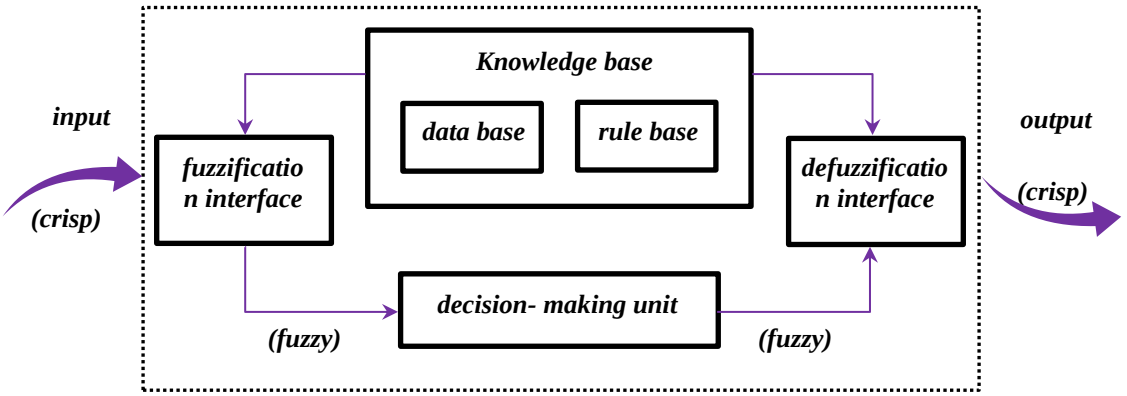

Figure 13. A fuzzy inference system.

- A rule base housing a set of fuzzy if-then rules.
- A database specifying the membership functions of the fuzzy sets utilized in the fuzzy rules.
- A decision-making unit executing the inference operations based on the rules.
- A fuzzification interface converting crisp inputs into degrees of match with linguistic values.
- A defuzzification interface converting the fuzzy outputs of the inference into a crisp output.

Typically, the rule base and the database are commonly referred to collectively as the knowledge base. The process of fuzzy reasoning in fuzzy inference systems involves the following steps:

1- Assessing the input variables against the membership functions on the premise section to derive the membership values (or compatibility measures) for each linguistic label. This stage is frequently termed fuzzification.

2- Merging the membership values on the premise section using a specific T-norm operator, typically multiplication or min., to determine the firing strength (weight) of each rule.

3- Producing the qualified consequent (either fuzzy or crisp) for each rule based on the firing strength.
4- Aggregating the qualified consequents to yield a crisp output. This process is known as defuzzification.

The ANFIS model, which integrates concepts from both fuzzy control and neural networks, combines the strengths of neural networks and fuzzy control systems. This approach enables the integration of the learning capabilities and computational power of neural networks into fuzzy control systems, while also incorporating the high-level reasoning capabilities of fuzzy control systems into neural networks. Essentially, neural networks can enhance their transparency to resemble fuzzy control systems more closely, whereas fuzzy control systems can adapt autonomously to resemble neural networks. Various methods have been proposed for partitioning the input space and addressing the structure identification problem. Essentially, ANFIS represents a graphical network depiction of a Sugeno-type fuzzy system, enriched with neural learning capabilities. The network comprises nodes with specific functions or roles organized into layers with designated functions. To exemplify the representational capabilities of ANFIS, the neural fuzzy control system under discussion is founded on Tagaki-Sugeno-Kang (TSK) fuzzy rules. In this framework, the consequent parts are formulated as linear combinations of their preconditions. The TSK fuzzy rules adhere to the following structure:

$$R^{j}: \text{IF } x_1 \textit{ is } A_1^j \text{ AND } x_2 \textit{ is } A_2^j \text{ AND}\ldots\text{AND } x_n \textit{ is } A_n^j \quad (3)$$
$$\text{THEN } y = f_j = a_0^j + a_1^j x_1 + a_2^j x_2 + \ldots + a_n^j x_n$$

where x_i (i = 1, 2, …, n) A_i^j are input variables (evaporation effecting factors), y is the output variable (daily evaporation measurements), are linguistic terms of the precondition part with membership functions $\mu_{A_i^j}(x_i)$ and a_1^j ЄR are coefficients of linear equations f_i (x_1, x_2, …, x_n) (j = 1, 2, ..., m, i = 1, 2, …, n). To streamline the discussion, let's narrow our focus to a particular neuro-fuzzy controller (NFC) known as an adaptive neural-based fuzzy inference system (ANFIS).

Assume that the fuzzy control system under consideration has two inputs x_1 and one output y and that the rule base contains two TSK fuzzy rules as follows:

$$R^{1}: \text{IF } x_1 \textit{ is } A_1^1 \text{ AND } x_2 \textit{ is } A_2^1 \text{ , THEN } y = f_1 = a_0^1 + a_1^1 x_1 + a_2^1 x_2 \quad (4)$$

$$R^{2}: \text{IF } x_1 \textit{ is } A_1^2 \text{ AND } x_2 \textit{ is } A_2^2 \text{ , THEN } y = f_2 = a_0^2 + a_1^2 x_1 + a_2^2 x_2 \quad (5)$$

In fuzzy logic approaches, for given input values x_1 and x_2, the inferred output y^* is calculated by:

$$y^* = (\mu_1 f_1 + \mu_2 f_2)/(\mu_1 + \mu_2) \quad (6)$$

Where μ_j are firing strengths of R_j (j = 1, 2), and are given by:

$$\mu_j = \mu_{A_1^j}(x_1) \times \mu_{A_2^j}(x_2) \qquad j = 1, 2 \tag{7}$$

If product inference is employed, the corresponding ANFIS architecture is depicted in figure 14, where the node functions within the same layers adhere to the following descriptions. Figure 1 is sourced from the reference book by Lin & Lee (1995). In this ANN architecture, each layer can be attributed with the following meanings:

Layer 1: Every node within this layer represents an input and merely transmits external signals to the subsequent layer.

Layer 2: Every node in this layer acts as a membership function $\mu_{A_i^j}(x_i)$, and its output specifies the degree to which the given x_i satisfies the quantifier A_i^j. Generally, $\mu_{A_i^j}(x_i)$ is selected as bell-shaped with a maximum equal to 1 and minimum equal to 0, such as:

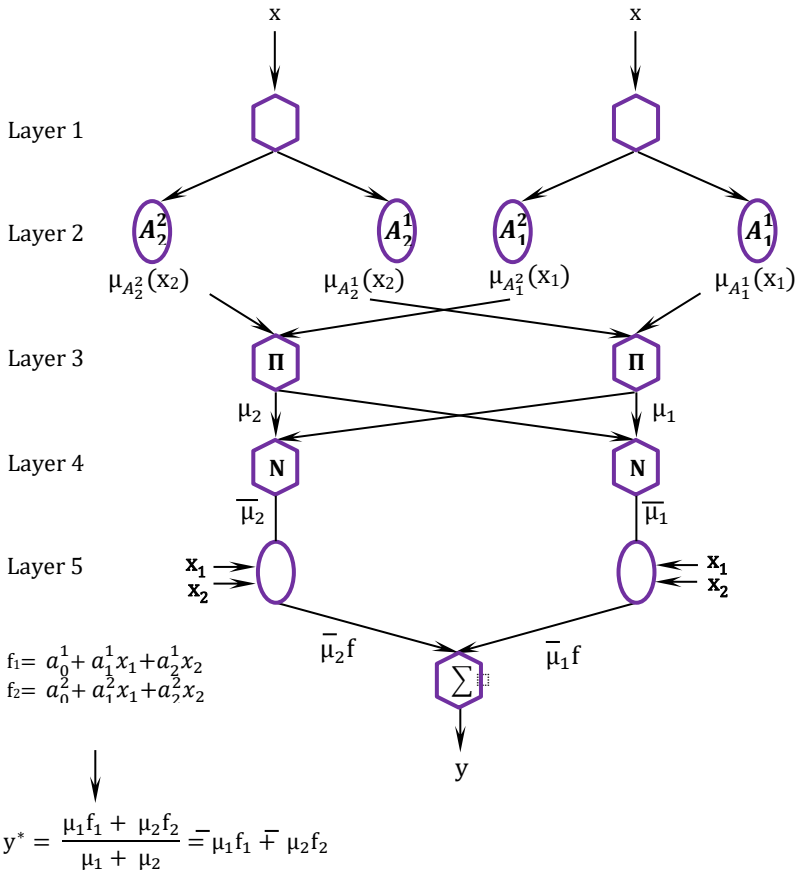

Figure 14. A fuzzy inference system.

$$\mu_{A_i^j}(x_i) = 1 \Big/ \left\{ 1 + \left[\left((x_i - m_i^j)/\sigma_i^j \right) \right]^2 \right\}^{b_i^j} \tag{8}$$

or

$$\mu_{A_i^j}(x_i) = \exp\left\{-\left[\left(\left(x_i - m_i^j\right)/\sigma_i^j\right)\right)^2\right]^{b_i^j}\right\} \quad (9)$$

where $\{ m_i^j, \sigma_i^j, b_i^j \}$ is the parameter set to be tuned. In fact, continuous and piecewise differentiable functions, such as the commonly employed trapezoidal or triangular membership functions, are also suitable candidates for node functions within this layer. The parameters within this layer are denoted as precondition parameters.

Layer 3: Every node in this layer is labelled Π and multiplies the incoming signals $\mu_j = \mu_{A_1^j}(x_1) \times \mu_{A_2^j}(x_2)$ and sends the product out. Each node output represents the firing strength of a rule.

Layer 4: Every node in this layer is labelled by N and calculates the normalized firing strength of a rule. That is the jth node calculates the ratio of the firing strength of the jth rule to that of all the rules as:

$$\overline{\mu_j} = \mu_j / \sum \mu \quad (10)$$

Layer 5: Every node j in this layer calculates the weighted consequent value as ;

$$\overline{\mu_j}(a_0^j + a_1^j x_1 + a_2^j x_2) \quad (11)$$

where $\overline{\mu_j}$ is the output of Layer 4 and $\{ a_0^j, a_1^j, a_2^j \}$ is the set to be tuned. Parameters in this layer are referred to as consequent parameters.

Layer 6: The only node in this layer is labelled as ∑, and it sums all incoming signals to obtain the final inferred result for the whole system (Lin & Lee, 1995).

Figure 15 shows resonant frequency estimation and error percentage when S21, S31, φ21 and φ31 as well as the changes in vias position are selected as inputs and ANFIS simulates the output data. The results here are not precise enough and hence less satisfactory.

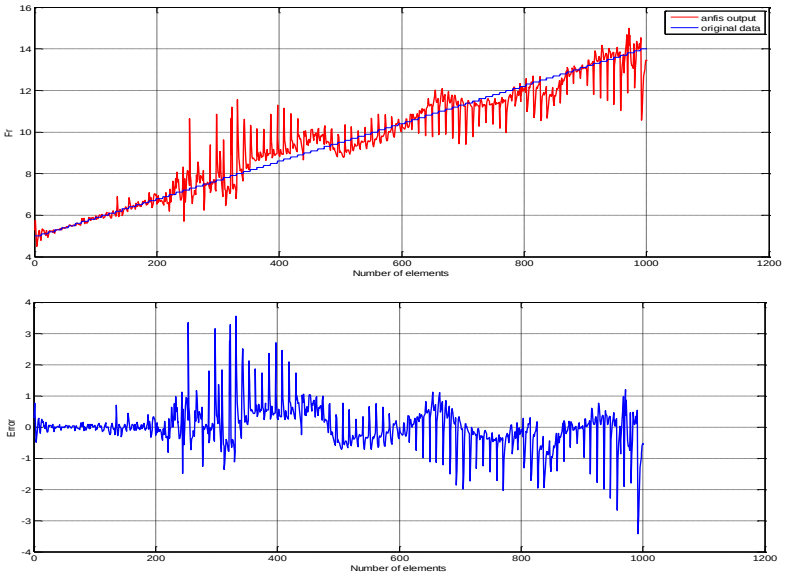

Figure 15. Resonant frequency estimation and its error using ANFIS.

Then S21 and S31 are predicted when resonant frequency and phases of two outputs as well as the position of vias are given as inputs. As can be seen from figure 16 and figure 17, the S-parameters can be recognized with a high accuracy and very low percentage of error.

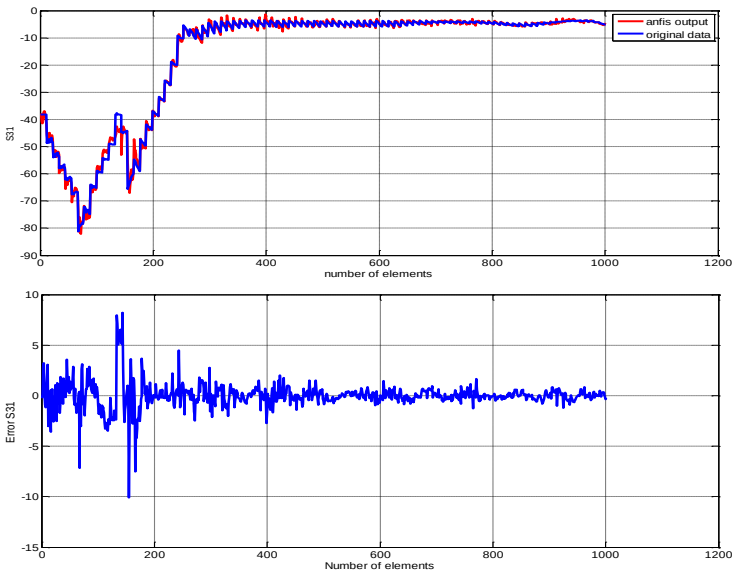

Figure 16. S31 parameters estimation and its error using ANFIS.

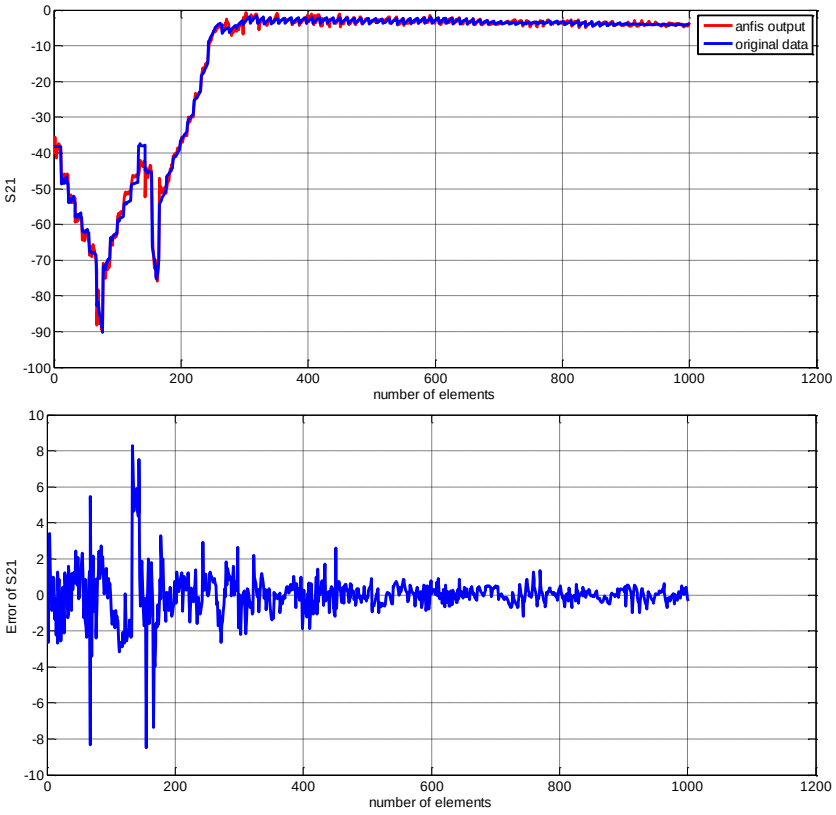

Figure 17. S21 parameters estimation and its error using ANFIS.

Finally, φ21, φ31 are predicted when resonant frequency and powers of the two outputs in addition to the position of vias are given as inputs. As can be seen from the figure 18 and figure 19, ANFIS fails to predict output phases appropriately.

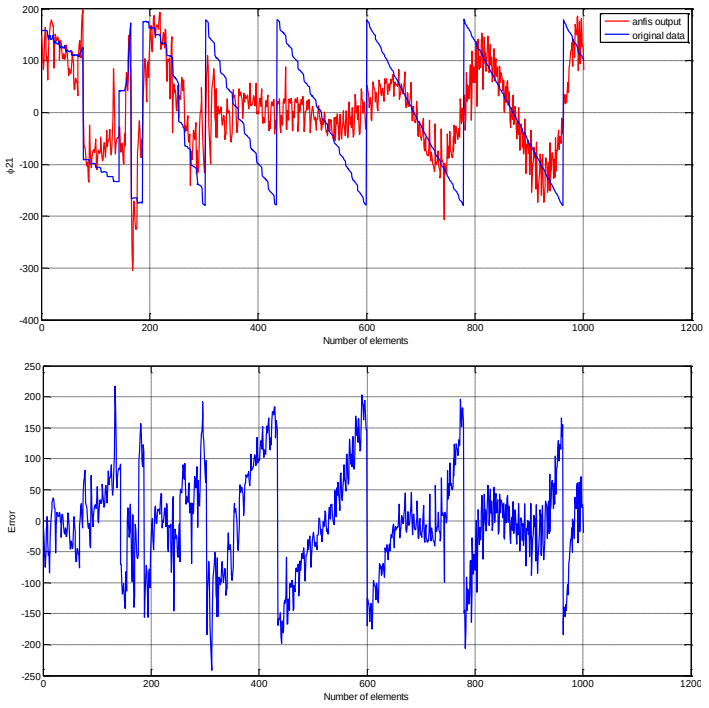

Figure 18. φ21 estimation and its error using ANFIS

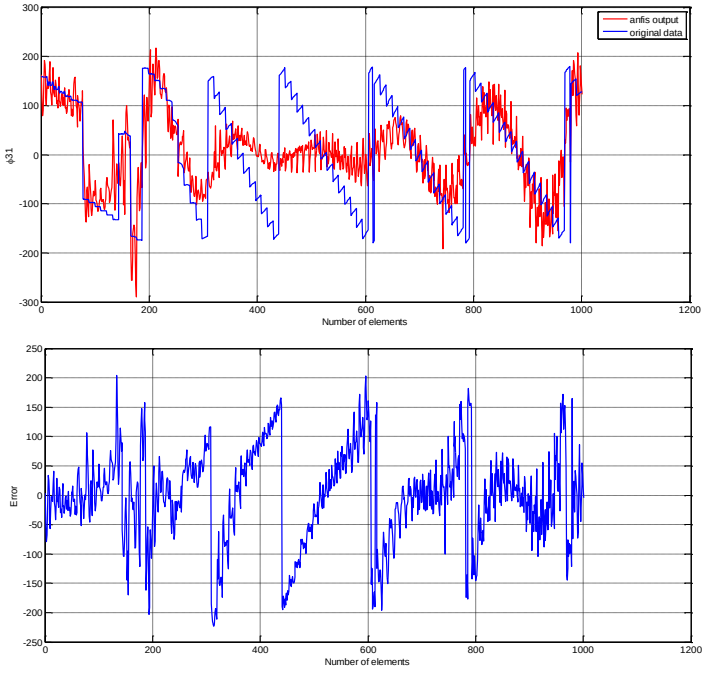

Figure 19. φ31 estimation and its error using ANFIS

3. CONCLUSION

Advanced machine algorithms such as neural networks and fuzzy logic systems have gained widespread recognition and have been extensively utilized across various engineering and scientific domains for numerous years. This paper focuses on calculating the resonant frequency, S-parameters, and output phases of a power divider constructed on a substrate integrated waveguide (SIW) structure with vias whose positions were shifted, resulting in asymmetry. To estimate these parameters, artificial neural networks and adaptive neuro-fuzzy inference systems were employed. The results indicate that ANFIS could predict S-parameters effectively, but the accuracy of output phases and resonant frequency prediction was limited. However, ANFIS results showed good agreement with experimental data, while other machine algorithms exhibited a high percentage of error due to either close proximity of input data or minimal differences in input values in some cases. It's worth noting that this method is not restricted to power dividers alone and can be easily applied to other microwave devices like phase shifters and antennas.

References

[1] E. J. Wilkinson, “An N-way hybrid power divider,” IRE Trans. Microwave Theory Tech., vol. MTT-8, pp. 116-118, Jan. 1960.
[2] L. I. Parad and R. L. Moynihan, “Split-tee power divider.” IEEE Trans. Microwave Theory Tech., vol. MTT-13, pp. 91-95, Jan. 1965.
[3] S. B. Cohn, “A class of broadband three-port TEM-mode hyhrjds,” IEEE Trans. Microwave Theory Tech., vol. MTT-16, pp. 110-116, Eeb. 1968.
[4] R. B. Ekinge, “A new method of synthesizing matched broad-hand TEM mode three ports,” IEEE Trans. Microwave Theory Tech., vol. MTT-19, pp. 81-88, Jan. 1971.
[5] A. M. Saleh, “Planar electrically symmetric N-way hybrid power dividers/combiners,” IEEE Trans. Microwave Theory Tech., vol. MTT-28, pp. 555-563, June 1980.
[6] D. Kother, B. Hopf, T. Sporkmann, and I. Wolff, “MMIC Wilkinson couplers for frequencies up to 110 GHz,” in IEEE MW-S Int. Microwave Symp.. Dig., pp. 663-666, 1995.
[7] Y. Wu, Y. Liu, Q. Xue, S. Li, and C. Yu, “Analytical design method of multiway dual-band planar power dividers with arbitrary power division,” IEEE Trans. Microw. Theory Techn., vol. 58, no. 12, pp. 3832–3841, Dec. 2010.
[8] Y. Wu, Y. Liu, and Q. Xue, “An analytical approach for a novel coupled line dual-band Wilkinson power divider,” IEEE Trans. Microw. Theory Techn., vol. 59, no. 2, pp. 286–294, Feb. 2011.
[9] F. Xu, G. Guo, E. Li, and J. Wu, “An ultra-broadband 3-dB power divider,” in Proc. 5th Global Symp. Millim. Waves (GSMM), May 2012, pp. 347–350.
[10] X. Wang, K.-L. Wu, and W.-Y. Yin, “A compact Gysel power divider with unequal power-dividing ratio using one resistor,” IEEE Trans. Microw. Theory Techn., vol. 62, no. 7, pp. 1480–1486, Jul. 2014.
[11] Abitrary power ratios and filtering responses using coupling structure,” IEEE Trans. Microw. Theory Techn., vol. 62, no. 3, pp. 431–440, Mar. 2014.
[12] L. Wu, Z. Sun, H. Yilmaz, and M. Berroth, “A dual-frequency Wilkinson power divider,” IEEE Trans. Microw. Theory Tech., vol. 54, no. 1, pp. 278–284, Jan. 2006.
[13] K.-K. M. Cheng and C. Law, “A novel approach to the design and implementation of dual-band power divider,” IEEE Trans. Microw. Theory Tech., vol. 56, no. 2, pp. 487–492, Feb. 2008.
[14] M.-J. Park and B. Lee, “A dual-band Wilkinson power divider,” IEEE Microw. Wireless Compon.Lett., vol. 18, no. 2, pp. 85–87, Feb. 2008.
[15] T. Yang, J.-X. Chen, and X. Y. Z. Xue, “A dual-band out-of-Phase power divider,” IEEE Microw. Wireless Compon.Lett., vol. 18, no. 3, pp. 188–190, Mar. 2008.
[16] Y. Wu, Y. Liu, and X. Liu, “Dual-frequency power divider with isolation stubs,” Electron. Lett., vol. 44, no. 24, pp. 1407–1408, Nov. 2008.
[17] Y. Wu, Y. Liu, Y. Zhang, J. Gao, and H. Zhou, “A dual band unequal Wilkinson power divider without reactive components,” IEEE Trans.
[18] Y.Wu,Y. Liu, and S. Li, “An unequal dual-frequency Wilkinson power divider with optional isolation structure,” Progr. Electromagn. Res., vol. 91, pp. 393–411, 2009.
[19] Xiaochuan Shen ; Yongle Wu ; Siyue Zhou ; Yuanan Liu,” A Novel Coupled-Line Tunable Wilkinson Power Divider With Perfect Port Match and Isolation in Wide Frequency Tuning Range,” IEEE Transactions on Components, Packaging and Manufacturing Technology (Volume: 6, Issue: 6, June 2016)
[20] Xiao-Lan Zhao; Li Gao, ; Xiu Yin Zhang ; Jin-Xu Xu,” Novel Filtering Power Divider With Wide Stopband Using Discriminating Coupling” IEEE MICROWAVE AND WIRELESS COMPONENTS LETTERS, VOL. 26, NO. 8, AUGUST 2016
[21] Eslamloo, Masoud Khoubroo, and Pejman Mohammadi. "Compact size, equal-length and unequal-width substrate integrated waveguide phase shifter." 2016 18th International Conference on Advanced Communication Technology (ICACT). IEEE, 2016
[22] Sagiroglu. S.: Guney, K.: Calculation of resonant frequency for an equilateral triangular microstrip antenna with the use of artificial neural networks. Microwave and Optical Technology LetI. 14(1997). 89-93.

[23] Sagiroglu. S.; Guney. K.; Erler, M.: Resonant frequency calculation for circular microstrip antennas using artificial neural networks. mt. J. of RF and Microwave Computer-Aided Engineering 8 (1998), 270-277.
[24] Guney. K.; Sagiroglu. S.; Erler. M.: Design of rectangular microstrip antennas with the use of artificial neural networks, Neural Network World 4 (2002). 361-370.
[25] Guney, K.; Sagiroglu, S.; Erler. M.: Generalized neural method to determine resonant frequencies of various microstrip antennas. mt. J. 01 RE and Microwave Computer-Aided Engineering 12 (2002). 131139.
[26] Yildiz, C.; Gultekin. S. S.; Guney. K.; Sagiroglu, S.: Neural models für the resonant frequency of electrically thin and thick circular microstrip antennas and the characteristic parameters of asymmetric coplanar waveguides hacked with a conductor. AEU-lnternational J. of Electronics and Communications 56(2002), 396-406.
[27] Guney. K.: Sarikaya, N.: Artificial neural networks for calculating the input resistance of circular microstrip antennas, Microwave and Optical Technology Lett, 37(2003), 107-111.
[28] Gultekin. S. S.; Guney. K.: Sagiroglu. S.: Neural networks for the calculation of bandwidth of rectangular n microstrip antennas. Applied computational Electromagnetics Society (ACES) Journal 18 (2003). 46-56.
[29] Guney, K.: Sarikaya, N.: Artificial neural networks for the narrow aperture dimension calculation of optimum gain pyramidal horns. Electrical Engineering 86(2004). 157-163.
[30] Karaboga, D.: Guney, K,: Sagiroglu. S.; Erler, M.: Neural computation of resonant frequency of electrically thin and thick rectangular microstrip antennas. lEE Proc. Mierow. Antennas Propagat. 146 (1999), 155-159.
[31] Sagiroglu, S.: Guney, K.; Erler, M.: Calculation of bandwidth for electrically thin and thick rectangular microstrip antennas with the use of multilayered pcrceptrons. Tnt. J. of RF and Microwave Compulter -Aided Engineering 9(1999), 277-286.
[32] Guney, K.; Erler, M,; Sagiroglu, S.: Artificial neural networks for the resonant resistance calculation of electrically thin and thick rectangular microstrip antennas, Electromagnetics 20(2000), 387-400.
[33] Guney. K.: Sagiroglu, S.: Erler. M.: Comparison of neural networks lhr resonant frequency computation of electrically thin and thick rectangular microstrip antennas. J. of Electromagnetic Waves and Applications 15 (2001), 1121—1145.
[34] K. Guney and N. Sarikaya, ‘‘Adaptive neuro-fuzzy inference system for the input resistance computation of rectangular microstrip antennas with thin and thick substrates’’, J. Electr. Wav. Appl., 18, pp. 23–39, 2004 .
[35] K. Guney and N. Sarikaya, ‘‘Adaptive neuro-fuzzy inference system for computing the resonant frequency of circular microstrip antennas’’, Appl. Comput. Electr. Soc. J., 19, pp. 188–197, 2004 .
[36] K. Guney and N. Sarikaya, ‘‘Computation of resonant frequency for equilateral triangular microstrip antennas using adaptive neuro-fuzzy inference system’’, Int. J. RF and Micr.
Comput.-Aid. Engin., 14, pp. 134–143, 2004 .
[37] K. Guney and N. Sarikaya, ‘‘Input resistance calculation for circular microstrip antennas using adaptive neuro-fuzzy inference system’’, Int. J. Infr. Millim. Wav., 25, pp. 703–716, 2004 .
[38] K. Guney and N. Sarikaya, “Adaptive neuro-fuzzy inference system for computing the resonant frequency of electrically thin and thick rectangular microstrip antennas’, International Journal of Electronics ,Volume 94, 2007 - Issue 9
[39] J.S.R. Jang, ‘‘Anfis: Adaptive-network-based fuzzy inference system’’, IEEE Trans. Syst., Man, Cyber., 23, pp. 665–685, 1993.
[40] M. EROL KESKIN , DILEK TAYLAN & ÖZLEM TERZI (2006) Adaptive neuralbased fuzzy inference system (ANFIS) approach for modelling hydrological time series, Hydrological Sciences Journal, 51:4, 588-598, DOI: 10.1623/hysj.51.4.588